Tracking of the phase change front of a PCM in a rectangular enclosure

Wito Plas, Wim Beyne, Kenny Couvreur, Michel de Paepe

Abstract

An experimental setup is designed to track the melting front of a phase change material, PCM, RT35HC, in a rectangular enclosure. One wall is heated through a constant heat flux, and another wall is kept at a uniform cold temperature, using a cold plate. All other walls are insulated in order to create a two-dimensional melt front. Photographs of the enclosure are taken every 20 seconds with a Basler Ace camera. Transient melting experiments have been performed. The effect of varying heat fluxes (800, 1000, 1200W/m²) has been investigated. Four different melting regimes are witnessed. Temperatures, measured by thermocouples inside the PCM are used to generate temperature contourplots, and an energy balance. A heat transfer coefficient over the melt is defined and compared to values found in literature. The four different melting regimes are still the same for the three different heat fluxes, but are initiated more quickly for a higher heat flux. By differentiating the liquid fraction in time, these melting regimes are defined. The energy balance over the enclosure is showing that the total added heat to the PCM is a function of liquid fraction. A heat transfer coefficient, based on this added energy to the enclosure follows the same trend as the differential liquid fraction. At the onset of natural convection in the enclosure, liquid fraction and thus also heat transfer rises fastest. Future CFD melting simulations can be done to compare these simulations to the experimental results.

Keywords: Phase Change Material, Experimental, heat transfer coefficient, visual measurement, Phase change front

1. Introduction

Thermal energy storage is necessary to make the transition to a fully sustainable world and to fill the gap between supply and demand for heat [1]. Latent heat storage, using phase change materials, PCMs, is able to store energy up to 240kJ/kg, which is 4 to 10 times more energy stored than through sensible heating per mass unit and up to 2 to 5 times per volume unit [1]. PCMs and latent heat storage systems are used in a wide variety of applications, due to their high energy density. Agyenim et al. and Lin et al. have given extensive lists of state of the art PCM applications [2,3].

Most PCMs possess low thermal conductivities, hampering heat transfer and loading times. During melting, natural convection can play a considerable role in enhancing the heat transfer [4]. The geometry of the enclosure (rectangular, cylindrical, etc.) has a major impact on these natural convection currents and the melting behaviour inside of the enclosure [2]. Only a limited amount of research has been done on the melting of PCMs in rectangular enclosures.

Studies about melting in rectangular enclosures can be split up into two different types of experiments, constant wall temperature, CWT and constant heat flux melting, CHF. An isothermal wall is obtained by circulating a hot fluid at constant temperature through tubes in a wall, made out of high thermal conductive materials, such as copper or aluminium. Constant heat flux experiments are performed by placing a heating element next to a high thermal conductive plate (aluminium, copper) and applying a constant voltage to the heater [7,8,9].

Melting in rectangular enclosures has been studied, as early as the 1980s. Early studies mainly focus on CWT melting, and one of the first to do so, are Viskanta et al [5] and Wolff and Viskanta [6], who studied the melting of low Prandtl number materials, such as gallium and tin. They are one of the first to define the different melting regimes in a rectangular enclosure. At first, there is the conduction regime; the melt front moves parallel to the hot plate. As more liquid melt is available, buoyancy driven (natural) convection becomes the dominant mode of heat transfer. Eventually natural convection starts to decrease again as more and more PCM has turned liquid. Liquid metals (low Prandtl) have high thermal conductivities and are excellent conductors of heat. Natural convection currents still play a significant role in the melting of the metals. Gallium and Tin are expensive materials however, and results from these studies are mainly used for benchmarking. More commonly used PCMs, such as paraffin waxes, lauric acids, fatty acids or other organic oil-derivatives have high Prandtl numbers [4,8,9,10]. Melting of these high Prandtl number PCMs occurs in the same fashion as the low Prandtl number PCMs and the same regimes of melting are witnessed in these CWT experiments [4,9]. A clear distinction between when these phases of melting occur, is however still missing.

Constant heat flux experiments have similar melting regimes, and temperature distributions as CWT experiments [7,8,9]. The temperature on the hot wall reaches a quasi-steady value after an amount of time, and melting in CHF experiments can therefore be seen as an equivalent CWT experiment [10]. Motahar et al. uses this heat flux applied to the enclosure to find a surface-averaged natural convection coefficient, by dividing the heat flux with a temperature difference, in particular the difference between wall temperature and melting temperature [7]. These convection coefficients in turn will be closer looked at in this paper.

Besides, the CHF and CWT experiments described before, there is a third, not so frequently used type. Hamad et al. uses a constant hot wall on one side, and a constant cold wall on the other side to study the effects of hot wall and cold wall temperatures on the melting of a fatty acid, PEG 1500 [10]. Melting patterns are similar to CWT and CHF experiments. The first derivative in time of the liquid fraction follows the same trend as the variation of Nusselt number in time, found by Wang et al. [9] and Kamkari et al. [4] in their CWT experiments. The rate of change of the liquid fraction in time, thus gives a good indication of the amount of heat that is being stored in the enclosure. This is an interesting claim which will be further investigated.

All of the previous mentioned experiments calculate transient heat transfer coefficients, or study transient melting behaviours. This experiment is set up to perform transient melting measurements, but with different boundary conditions; a constant heat flux to one side of the enclosure and a constant temperature on the other side. This approach also offers the possibility of steady-state measurements. Liquid fractions in time are compared to stored energy in the transient melting case, to further investigate the claims of Hamad [10]. Additionally, different heat transfer coefficients are calculated and compared to values found from literature.

2. Materials and method

2.1. Experimental apparatus

The experiment is designed to track the melting front in a rectangular enclosure. One vertical side is heated by constant heat flux and the opposing side is kept at a constant temperature. A schematic overview of the set-up is given in Figure 1.

The phase change material used in this experiment is RT35HC from the Rubitherm catalogue [11]. Properties of RT35HC are listed in Table 1. RT35HC has been selected as it has a narrow melting temperature range of 2°C and a transparent liquid melt. Additionally, there are lower thermal losses to the environment, by choosing a melting temperature not too high above the ambient temperature.

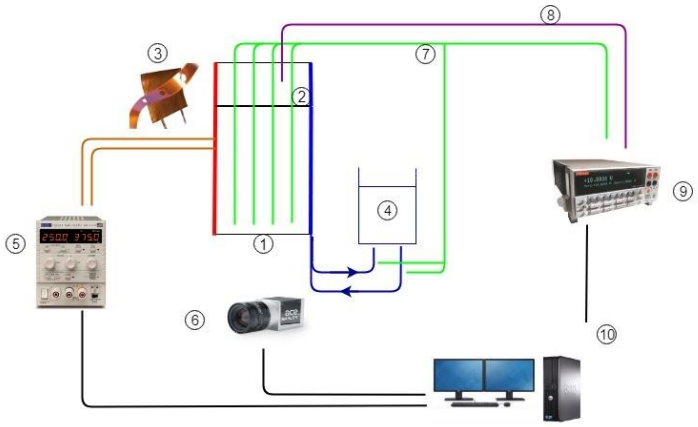

Figure 1: Schematic overview of set-up (1: PCM, 2: air, 3: heater, 4: constant temperature bath, 5: power source, 6: camera, 7: thermocouples, 8: pressure sensor, 9: Keithley, 10: computer

Table 1: RT35HC properties, as given by manufacterer

	Value	**Units**
Latent heat of fusion, L	240,000	J/kg
Specific heat capacity, Cp	2	kJ/kgK
Melting temperature, Tm	35	°C
Thermal conductivity (solid, liquid)	0.2	W/mK
Density solid/liquid	880/770	Kg/m³
Maximum operating temperature	70	°C

The enclosure is designed to accurately track the melting front in a rectangular enclosure, by limiting the thermal losses to the environment as much as possible. Walls of the enclosure consist of a transparent polycarbonate material, called Makrolon, which approximately has the same thermal conductivity as the PCM. Thickness of the Makrolon plates is 10mm. In front of the enclosure, a double glass wall was installed, with an air gap of 15 mm to minimize losses to the environment and still allowing visual measurements. The remaining walls are insulated with 3 cm thick polyurethane plates and can be assumed adiabatic. The enclosure is built up modularly, allowing for easy disassembly and removal of damaged parts. The top and bottom plates are attached via 8 and 10 bolts respectively to 4 Makrolon plates, which are glued together, as seen in Figure 2.

A Watlow heater was attached to an aluminium plate, 85 mm wide, 145 mm high and 3 mm thick. This heater has a maximum heating power of 75W. The heater is attached to a DC power source, PLH-120-P from Aim and Thurlby Thandar Instruments, which has a maximal power rating of 90W.

In order to reach steady state, a cold plate from Lytron at constant cold temperature was installed at the other side of the enclosure. The Temperature of the cold plate was kept at the same uniform value by a chiller, Julabo FL601. In transient experiments, this chiller was held at a temperature just below the melting point, 34°C, to guarantee that all PCM is able to melt at the cold plate side. In steady state experiments, this temperature is held sufficiently below the PCM melting temperature to guarantee that a solid state can coexist together with a liquid state.

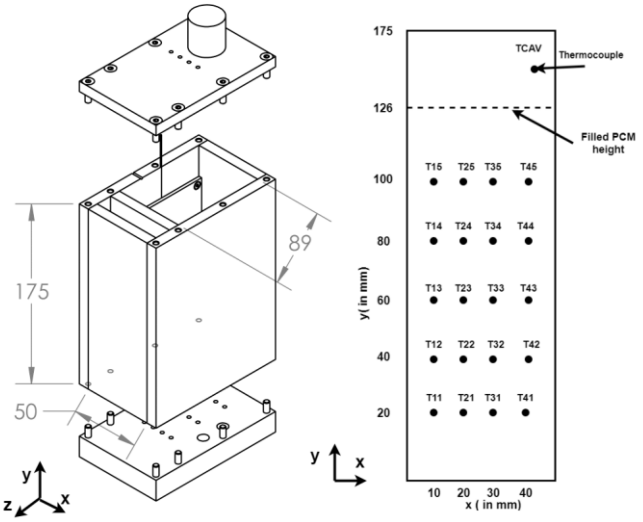

Figure 2: Geometry of enclosure and thermocouple positions

2.2. Procedure

The liquid melt is determined visually by periodically taking photo's at the front position of the enclosure, using a camera from Basler, acA2500-60um with lens TS1214-MP. Matlab image processing toolbox is used to process the images. Firstly, the images are cropped so that they only show the PCM. They are then converted to grey-scale images and are finally converted to binary images. A one corresponds with a white pixel, or solid and a zero with black or liquid melt. By counting the total amount of white pixels, solid fraction is calculated. The liquid percentage is then one minus this value, Equation 1. The cropped image has a resolution of 1678 pixels by 666 pixels in a viewing area of 50 by 126mm. Liquid PCM has a lower density than solid PCM and takes in more volume than solid PCM. By keeping the pixel ratio fixed, the obtained ratio in fact is thus the fraction of liquid PCM mass versus total PCM mass.

$$\frac{V}{V_0} = 1 - \frac{NP_1}{NP} \tag{1}$$

20 K-type thermocouples are used to measure temperatures inside the PCM and 11 K-type thermocouples are used to measure temperatures outside of the enclosure. To measure the maximum PCM temperature, three thermocouples are placed at equal distances at the back end of the heater. Two thermocouples are measuring the cold plate's in-and outgoing temperatures. One thermocouple measures the temperature inside the air void in the enclosure. Two thermocouples at heater side, two thermocouples at the back side of enclosure and one thermocouple is placed on top of the insulation plates to measure heat losses to the environment. The 20 K-type thermocouples inside the PCM are arranged as shown in Figure 2.

Thermocouple data is acquired, using a Keithley 2700, which is connected to a PC. Labview programming environment is used to communicate with the Keithley device, the power source and the camera.

Before the start of each experiment, water is sent through the cold plate tubes at a temperature of 34°C to guarantee a uniform initial temperature of the solid PCM. This initial temperature is chosen to be close to the melting point of the PCM to limit sensible heating.

The enclosure is gradually filled layer by layer. When the liquid melt cools down, it shrinks in volume. This shrinkage is not proportional to the noticed volume change, meaning air is still trapped inside the solid PCM. When PCM melts, liquid PCM will fill up these cavities, thus not accurately representing liquid fractions.

Empty mass of the enclosure is measured as well as filled enclosure mass. This way the mass of the PCM in the enclosure can be accurately calculated. Knowing the volume of PCM in the enclosure, PCM densities in the enclosure are calculated, which are shown in Table 2Table 1.

Table 2: empty and filled mass of enclosure

Empty enclosure	Filled enclosure	Density
2.116kg	2.585kg	837kg/m³

3. Results and discussion

3.1. Melt front position

The effect of varying heat fluxes (800, 1000 and 1200 W/m²) on the amount of liquid PCM and on the heat transfer coefficient are investigated. All other parameters, such as cold plate temperature and initial temperature are held constant at a temperature of 34°C, right below the melting temperature of the PCM.

Solid-liquid interface lines for the three heat fluxes are **displayed** in Figure 3. These contour lines have small deviations in the bottom left corner. This deviation occurs, due to a small but negligible PCM leak in front of the enclosure. No big variations in PCM volume are witnessed in between experiments, and the influence of the leak can be assumed negligible. The farther away two contour lines are from each other, the more PCM is molten in that time step. These melting contour lines are similar to the ones found in literature [4,8,10].

At first, conduction is dominant and there is a vertical melt front. This regime is followed by a transition region, where conduction and natural convection both play an almost equal role. The melt front starts to become more skewed. As more PCM is molten natural convection takes over entirely, this is the third regime. The melt front is now almost everywhere diagonal. Finally, the last regime is entered, where natural convection is the main mode of heat transfer, most of the PCM is already molten and melting rates are decreasing. The solid PCM has a triangular shape.

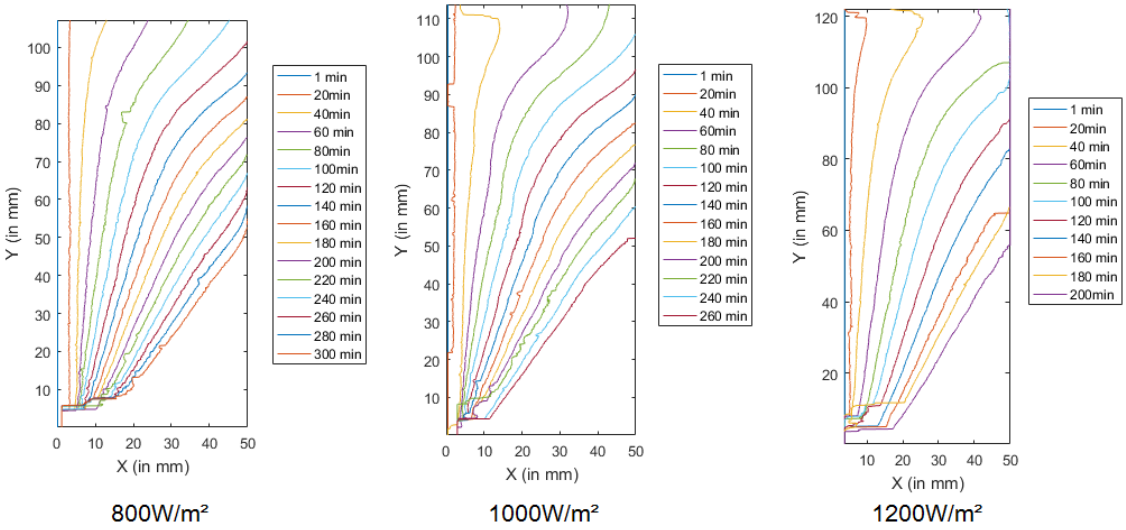

Figure 3Melt front contours

Using Equation 1, liquid fractions are calculated and are presented in Figure 5. A higher heat flux corresponds with faster melting. These liquid fractions in time, first follow a linear curve, depending on the heat flux that is being applied. After 80-90 minutes, these start to bend however and melting slows down, this is the same point as where the melt front reaches the other side of the wall. For the 800W/m² case this is at a later time than for the 1200W/m² case. There are two reasons for the slowing down of the melting of the PCM. A first reason, is that after this point,

the liquid PCM is in direct contact with the cold plate and heat is now also directly being transferred to the cold plate. Secondly, the solid-liquid line, along where the PCM is melting, starts to decrease in length [10].

3.2. Hot wall temperature and convection coefficients

This experiment is set up to be a constant heat flux experiment, but, depending on the heat flux, temperature of the hot wall reaches a quasi-steady value after 60 minutes, see Figure 6. It rises quickly at first and attains a quasi-steady value after about 60 minutes. This can be best understood, when looking at the simplified 1-dimensional heat transfer equation, with two heat resistances in parallel (conduction and convection), defined in Equation 2. h_{conv}, is the natural convection coefficient in the liquid, k, the thermal conductivity and l, the length of the liquid PCM. Sensible heating of the solid PCM is neglected, and the melt front is at a uniform temperature, T_m. Initially, l is very small and h_{conv} is almost non-existent as there is not enough liquid PCM to start natural convection. k/l is the dominating heat transfer factor (conduction) in the equation. Since q is held constant, the temperature difference, $T_w - T_m$ must rise as l rises. As more and more PCM starts to melt however, (buoyancy driven) natural convection is becoming the main mode of heat transfer. k/l is no longer the dominating factor in the equation, but h_{conv} is. This natural convection coefficient takes a quasi-constant value and the temperature difference,$T_w - T_m$ stabilises in time.

$$\dot{q} = \left(h_{conv} + \frac{k}{l}\right)(T_w - T_m) \tag{2}$$

If the foregoing discussion is valid, an increase in heat flux should result in an increase in T_w. Plotting the quasi-steady value of the hot wall temperature, after 100 minutes to 6 different heat fluxes (200, 300, 400, 800, 1000, 1200 W/m²) already gives more backing for this claim, see Figure 4. A linear regression curve is also plotted in this graph and is given by Equation 3. Maximum deviation between start and stop of the steady-state hot wall temperature is 0.5K. The intercept of this equation lies very close to the melting temperature.

$$T_w = 0.01715\,\dot{q} + 34.81 \tag{3}$$

The heat transfer coefficient, defined by Motahar et al. (Equation 4) is used to measure the heat transfer coefficient over the liquid PCM. This in fact is the parallel thermal resistance of the natural convection and the conduction through the liquid PCM ($h_{conv} + k/l$). This heat transfer coefficient is plotted for the three different heat fluxes of 800, 1000 and 1200W/m² in Figure 7. The initial PCM, and the wall temperature is at a temperature below the melting temperature. As

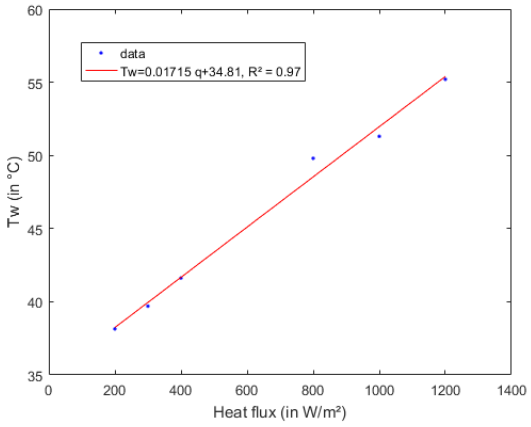

Figure 4Wall temperature in function of heat flux

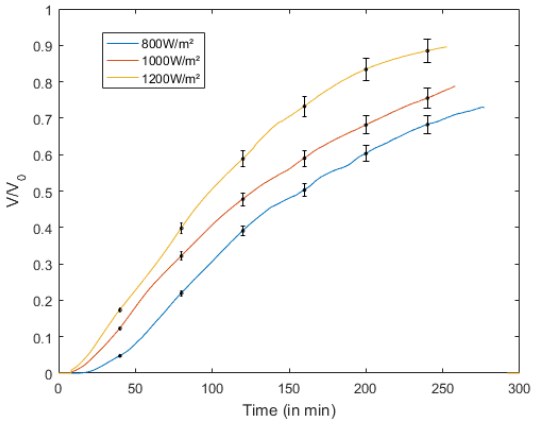

Figure 5Liquid fractions for three heat fluxes

the hot wall will reach the melting temperature, melting starts to occur and the heat transfer coefficient first goes to infinity. This graph starts after 30 minutes, as heat transfer by natural convection is starting to dominate the

heat transfer. As time progresses, and hot wall reaches equilibrium, this coefficient goes to a steady value of around 64.7 $\pm$ 5.9 W/m²K.

$$h = \frac{\dot{q}}{T_w - T_m} \tag{4}$$

3.3. Temperature distribution, stored energy and its relation to the convection coefficient

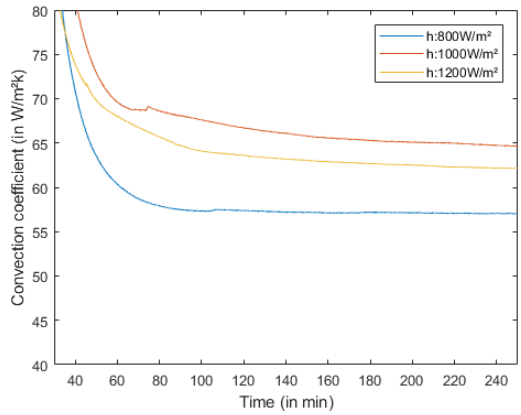

Figure 7:Heat transfer coefficients in function of time

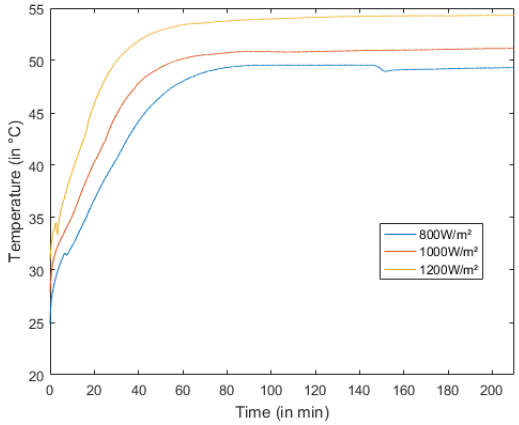

Figure 6:Wall temperature in function of time

Temperature contourplots can be used to gain further insight in the melting of the PCM. In order to not overload the results too much, only the results for the 1000W/m² case are shown. Liquid volume fractions of the 1000W/m² case follow the same trend as the 800 and the 1200W/m² cases. Temperature contourplots for the 1000W/m² case are shown in Figure 8. The contourplots do not show clear lines of melting. This is because the thermocouples have shifted from their original positions. In the last contourplot, it is nonetheless possible to see that hot liquid PCM rises to the top, giving way to stratified layers of hot PCM, hampering the natural convection flow [4].

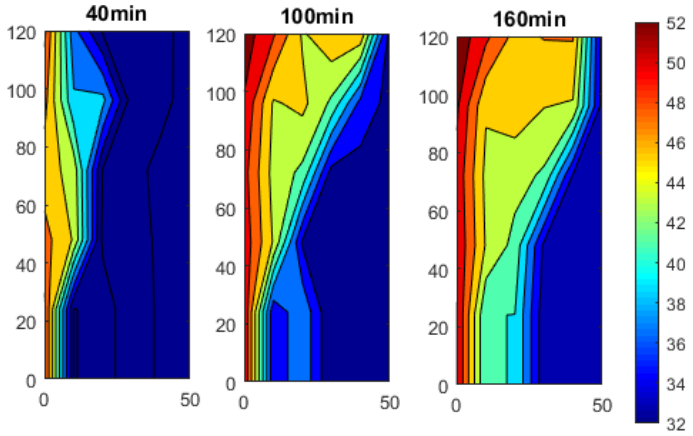

Figure 8 Temperature contourplot

Using the data from the thermocouples and the liquid fractions from the camera, an energy balance over the enclosure for the 1000W/m² case is made. Latent, sensible and total energy stored in the PCM are calculated, using Equation 5. Liquid volume fraction, χ, is calculated, using the visual method. T_{liq} is the average PCM temperature of all the thermocouples present in the melt at that time. Q_{in}, is the electrical energy supplied to the PCM. Q_{out}, is the energy transferred to the cold plate. Q_{loss} is the loss to the environment and L is the specific latent heat of energy of the PCM. The energy balance over the enclosure is shown in Figure 9.

$$Q_{in}(t) = m\,\chi\,L + m\chi(T_{liq} - T_{ini}) + Q_{out} + Q_{loss} \quad (5)$$

The average liquid temperature takes an asymptotic value after 60-80 minutes, indicating once again that the thermal resistance over the liquid is not so big, and that natural convection is the main mode of heat transfer. Heat stored in the form of latent energy, is a lot bigger than heat stored in the form of sensible energy. Total heat, being absorbed by the PCM follows the same trend, as the volume fraction in time (Latent heat line in the graph).

Now that the energy balance over the enclosure is made, a CWT heat transfer coefficient can be calculated [4,9] see Equation 6. When looking more closely to this heat transfer coefficient, this equation can be rewritten and simplified.

$$\bar{h} = \frac{Q(t+\Delta t) - Q(t)}{\Delta t (T_w - T_m) A_w} \cong \frac{\chi(t+\Delta t) - \chi(t)}{\Delta t} \cdot \frac{mL}{\left((T_w - T_m) A_w\right)} \quad (6)$$

Since the total stored energy inside the enclosure is closely related to the liquid fraction, χ, and by omitting the sensible heating of the liquid PCM and the losses to the cold plate and to the environment, Equation 5 is reduced to $Q \cong m\,\chi\,L$. This heat transfer coefficient is primarily used in CWT experiments, where the hot wall temperature is held constant. The second factor in Equation 6 therefore is also a constant. This heat transfer coefficient is actually the first derivative in time of the liquid fraction multiplied with a constant. The first derivative in time of the liquid fraction is also calculated by the author Hamad et al [10] (CHF experiment) and follows the same trend as the previously defined heat transfer coefficient. It follows that the first derivative in time of the liquid fraction therefore is an excellent indicator that can qualitatively describe the heat transfer to and inside the enclosure for CWT experiments. This is a CHF experiment, but the hot wall temperature reaches a quasi-constant value after 40-50 minutes. The derivative of the liquid fraction is therefore also calculated in this work.

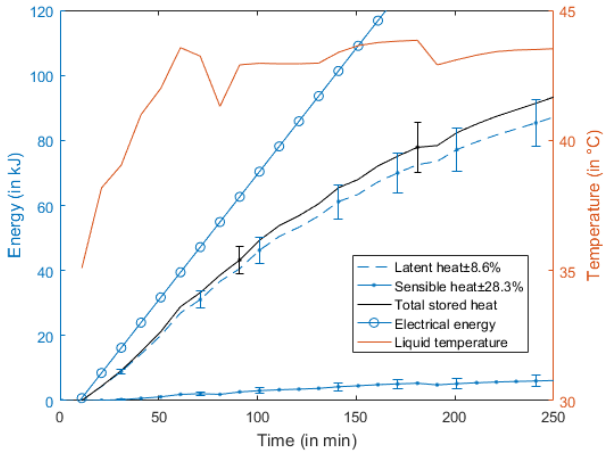

Figure 9: Energy distribution and average temperature

3.4. Time derivative of liquid fractions

Taking the derivative in time of these melt fractions allows for a better defining of the melting regimes. Liquid fraction derived in time is given by Equation 7 and is shown in Figure 10.

$$\frac{d\chi}{dt} = \frac{\chi(t+\Delta t) - \chi(t)}{\Delta t} \quad (7)$$

At first, there is slow melting in the conduction regime (I, 0-14min), melt front stays parallel to the hot wall. Heat transfer is low and only occurs through conduction. As more liquid PCM is available, natural convection starts and melting rates increase (II, 14-48min). This is the transition regime, where conduction and convection both play a role. The melt front is now starting to take a more skewed form, away from the hot surface. After 48 minutes, main mode of heat transfer is through natural convection and melting rates are at a peak (III,48-90). The melt front reaches the

other side of the enclosure. Heat is now also transferred to the cold plate, the solid-liquid line starts to shrink again and melting rates are lowering (IV, 90-end).

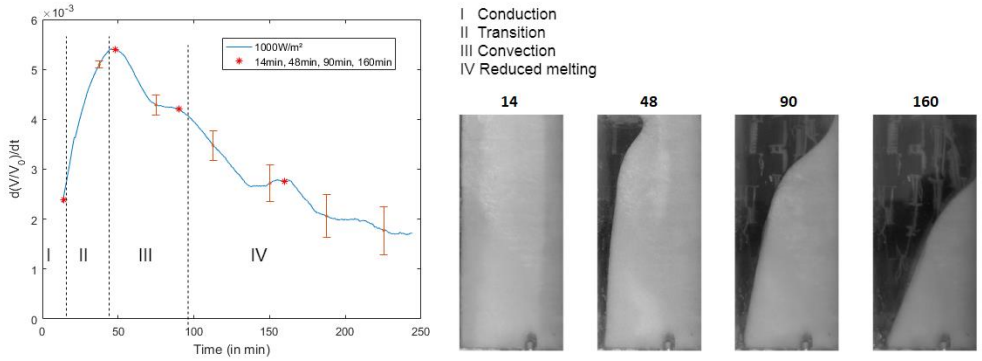

Figure 10: Differential liquid fraction

4. Conclusions

A rectangular enclosure is made, capable of performing three types of experiments, transient melting, solidification and steady-state of which only the transient case is shown in this paper. Four different melting regimes are witnessed in the transient regime. Liquid melt fractions and contours are similar to values found in literature. (Constant heat flux) heat transfer coeffcients in the liquid melt take a quasi-constant value of about 60 $\pm$5 W/m²K, regardless of heat flux. The comparison is made between the convection coefficients calculated, using the constant hot wall approach and the constant heat flux approach. Furthermore, it is found that the first derivative in time of the liquid fraction in time offers a good approximation for the (constant wall temperature) heat transfer coefficient.

Nomenclature

A	[m²]	Area
Cp	[J/kgK]	Specific heat capacity
h	[W/m²K]	Heat transfer coefficient (CHF)
$\overline{h}$	[W/m²K]	Heat transfer coefficient (CWT)
H	[m]	Characteristic length
k	[W/mK]	Thermal conductivity
l	[m]	Liquid length
L	[J/kg]	Latent heat of fusion
m	[kg]	Total mass of PCM
Nu	[-]	Nusselt number
Q	[J]	Energy
$\dot{q}$	[W/m²]	Heat flux
T	[°C / K]	Temperature
χ	[-]	Liquid Fraction
Δt	[s]	Time difference
t	[s]	Time

subscripts

conv	convective
w	wall
m	melt
ini	initial
out	out
loss	loss
liq	liquid
1	solid pixel
0	liquid pixel

Abbreviations

PCM	Phase change material
NP	Number of pixels
CHF	Constant heat flux
CWT	Constant wall temperature

References

[1] A. F. Regin, S. C. Solanki, and J. S. Saini, “Heat transfer characteristics of thermal energy storage system using pcm capsules: A review, “Renewable and Sustainable Energy Reviews, vol. 12, no. 9,pp. 2438–2458, 2008.

[2] M. M. Alkilani, K. Sopian, M. A. Alghoul, M. So-hif, and M. H. Ruslan, “Review of solar air col-lectors with thermal storage units, “Renewable and Sustainable Energy Reviews, vol. 15, no. 3,pp. 1476–1490, 2011

[3] Z. Gu, H. Liu, and Y. Li, “Thermal energy recovery of air conditioning system heat recovery system calculation and phase change materials development,”Applied Thermal Engineering, vol. 24,no. 17, pp. 2511–2526, 2004.

[4] S. C. Fok, W. Shen, and F. L. Tan, “Cooling of portable hand-held electronic devices using phase change materials in finned heat sinks, “International Journal of Thermal Sciences, vol. 49, no. 1,pp. 109–117, 2010.

[5] R. Baetens, B. P. Jelle, and A. Gustavsen, “Phase change materials for building applications: A state-of-the-art review, “Energy and Buildings, vol. 42, no. 9, pp. 1361–1368, 2010.

[6] W. Lu and S. A. Tassou, “Characterization and experimental investigation of phase change materials for chilled food refrigerated cabinet applications, “Applied Energy, vol. 112, pp. 1376–1382,2013

[7] . Y. Kim, B.-S. Hyun, J.-J. Lee, and J. Rhee, “Numerical study of the spacecraft thermal control hardware combining solid liquid phase change material and a heat pipe, “Aerospace Science and Technology, vol. 27, no. 1, pp. 10–16, 2013

[2] F. Agyenim, N. Hewitt, P. Eames, and M. Smyth, “A review of materials, heat transfer and phase change problem formulation for latent heat thermal energy storage systems (lhtess),”Renewable and Sustainable Energy Reviews, vol. 14, no. 2,pp. 615–628, 2010.

[3] Y. Lin, Y. Jia, G. Alva, and G. Fang, “Review on thermal conductivity enhancement, thermal properties and applications of phase change materials in thermal energy storage, “Renewable and Sustainable Energy Reviews, vol. 82, pp. 2730–2742, 2018

[4] H. Shokouhmand and B. Kamkari, “Experimental investigation on melting heat transfer characteristics of lauric acid in a rectangular thermal storage unit, “Experimental Thermal and Fluid Science, vol. 50, pp. 201–212, 2013.

[5] C. Gau and R. Viskanta, “Melting and solidification of a pure metal on a vertical wall, “Journal of Heat Transfer, vol. 108, no. 1, pp. 174–181, 1986.

[6] F. Wolff and R. Viskanta, “Solidification of a pure metal at a vertical wall in the presence of liquid superheat, “International Journal of Heat and Mass Transfer, vol. 31, no. 8, pp. 1735–1744,1988.

[7] S. Motahar, A. A. Alemrajabi, and R. Khodabandeh, “Experimental investigation on heat transfer characteristics during melting of a phase change material with dispersed tio2 nanoparticles in a rectangular enclosure, “International Journal of Heat and Mass Transfer, vol. 109, pp. 134–146,2017.

[8] M. H. Joneidi, M. J. Hosseini, A. A. Ranjbar,and R. Bahrampoury, “Experimental investigation of phase change in a cavity for varying heat flux and inclination angles, “Experimental Thermal and Fluid Science, vol. 88, pp. 594–607, 2017.

[9] Y. Wang, A. Amiri, and K. Vafai, “An experimental investigation of the melting process in a rectangular enclosure, “International Journal of Heat and Mass Transfer, vol. 42, no. 19, pp. 3659–3672,1999

[10] F. A. Hamad, E. Egelle, K. Cummings, andP. Russell, “Investigation of the melting processof polyethylene glycol 1500 (peg 1500) in a rectangular enclosure, “International Journal of Heat and Mass Transfer, vol. 114, pp. 1234–1247, 2017.

[11] Rubitherm Technologies GmbH,RT35HC, 12015.